14IND03 Deliverable D4

Grant Agreement number	14IND03
Project short name	StrengthABLE
Deliverable Reference Number and Title	D4 ISO14577-2 compatible calibration and verification report for the MEMS based IIT system that will bridge the length and force-scale (<1 µm to ~10 µm, 1 µN to ~few hundred µN) between AFM and nanoindentation
Organisation Name of Lead Partner	Adama
Due Date of the Deliverable	May 2017
Actual Submission Date of Deliverable	March 2018

Note: Nanomechanical characterization of soft materials using a micro-machined nanoforce transducer with an FIB-made pyramidal tip

Z. Li, S. Gao, U. Brand, K. Hiller, N. Wollschläger, and F. Pohlenz

Note: Nanomechanical characterization of soft materials using a micro-machined nanoforce transducer with an FIB-made pyramidal tip

Z. Li,[1,a)] S. Gao,[1] U. Brand,[1] K. Hiller,[2] N. Wollschläger,[3] and F. Pohlenz[1]

[1]*Phyikalisch-Technische Bundesanstalt, 38116 Braunschweig, Germany*
[2]*Technische Universität Chemnitz, 09126 Chemnitz, Germany*
[3]*Bundesanstalt für Materialforschung und -Prüfung, 12205 Berlin, Germany*

The quantitative nanomechanical characterization of soft materials using the nanoindentation technique requires further improvements in the performances of instruments, including their force resolution in particular. A micro-machined silicon nanoforce transducer based upon electrostatic comb drives featuring the force and depth resolutions down to ~1 nN and 0.2 nm, respectively, is described. At the end of the MEMS transducer's main shaft, a pyramidal tip is fabricated using a focused ion beam facility. A proof-of-principle setup with this MEMS nanoindenter has been established to measure the mechanical properties of soft polydimethylsiloxane. First measurement results demonstrate that the prototype measurement system is able to quantitatively characterize soft materials with elastic moduli down to a few MPa. *Published by AIP Publishing.* [http://dx.doi.org/10.1063/1.4977474]

The well-standardized nanoindentation technique[1,2] is included in the favorable approaches to the nanomechanical characterization of materials in small volumes. Especially for hard materials with typical elastic moduli $E \gg 1$ GPa, nanoindentation instruments[3] equipped with sharp pyramid-like tips (e.g., Berkovich and Vickers) have proven to work well. For soft materials with E down to less than several MPa,[4] however, they generally fail to perform measurement with a Berkovich/Vickers tip, mainly because of the limited force resolution. In some cases, large spherical indenters[5,6] (e.g., tip radii from tens to hundreds of μm) can help to extend the functionality of a nanoindentation instrument, but they lead, unfortunately, to the loss of the lateral resolution of the measurement.

Atomic force microscopes (AFMs) have long been applied for the nanomechanical characterization of soft materials,[7–9] owing to their high force, depth/deflection, and lateral resolutions. However, quantitative AFM nanomechanical measurements suffer generally practical problems,[10,11] including nonlinearity in the case of large cantilever deflection, difficulties in the quantitative characterization of the AFM tip area function, zero-contact point detection, long-term tip stability, and so on.

For the quantitative nanomechanical characterization of soft materials with the nanoindentation technique, it is therefore highly desired that the measurement system should feature high force and displacement sensitivities, large indentation depth, stable and reliable indenter tip ready for quantitative characterization, seamless application of the standardized system calibration, and data evaluation methods. To satisfy the aforementioned demands, a MEMS-based nanomechanical measurement system is proposed in this paper.

As shown in Fig. 1(a), a bi-directional MEMS transducer has been developed on the basis of a lateral electrostatic comb-drive actuation mechanism.[12] The main shaft of the transducer is symmetrically suspended by folded springs. A set of comb drives with a number of finger pairs is designed to move the main shaft in the direction of the +z-axis (symmetry axis of the transducer). The electrostatic force F_e generated by the comb drives[12] is

$$F_e = N \cdot \varepsilon \cdot \frac{t}{g} \cdot U_Z^{+2}, \tag{1}$$

where N is the number of finger pairs for the indentation test, ε the permittivity in air, U_z^+ the DC drive voltage applied to the comb drives, t the finger height, and g the gap between movable and fixed fingers, as shown in Fig. 1(b). The actual indentation force applied to the surface of a specimen under test is

$$F_{\text{indent}} = F_e - k_z \cdot h_{\text{indent}}, \tag{2}$$

where h_{indent} is the penetration depth beneath the specimen surface,[1] and k_z the effective spring constant of the MEMS suspending springs along its moving axis.

Another set of comb drives was implemented in the transducer for generating the pull-off forces to lift the MEMS shaft. This force is controlled by the DC signal U_z^-.

To measure the in-plane displacement of the transducer with a capacitive sensing technique, a sinusoidal signal with the frequency $f_{\text{sin}} = 60$ kHz is added to the signals U_z^+ and U_z^- with inversed phase, respectively. The output AC current from the transducer is converted to a voltage signal by a home-made I/U converter and then sent to a lock-in amplifier (SR830, Stanford Research Systems) for further processing. Careful design of the dual-directional comb drives within the transducer ensures that the lock-in output V_s is linearly proportional to the axial movement of the transducer's main shaft.

a)Author to whom correspondence should be addressed. Electronic mail: zhi.li@ptb.de.
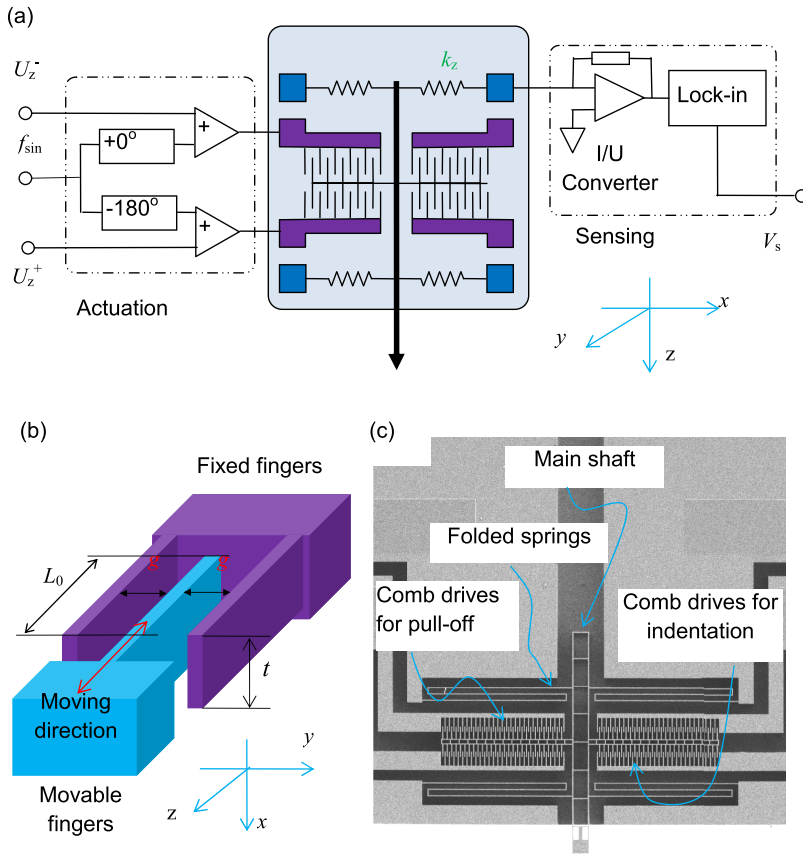
FIG. 1. (a) Schematic of the electrostatic MEMS transducer and the fundamental principle of the drive and sensing system for this transducer. (b) 3D illustration of the finger pairs. (c) SEM image of the MEMS transducer (without pyramidal tip).

The designed MEMS transducer has been fabricated by using silicon bonding deep reactive-ion etching (DRIE) technology[13] on (100) p-type (B-doped) silicon wafers with a resistivity of 0.01-0.05 Ω cm. The comb finger height and finger gap (shown in Fig. 1(b)) are $t = 50$ μm and $g = 3$ μm, respectively. One of the prototypes is illustrated in Fig. 1(c). Here, the number of finger pairs for indentation/pull-off is $N = 56$, leading to a maximum output electrostatic force F_e up to 40 μN at $U_z^+ = 70$ V. And the maximum in-plane displacement of the transducer at null-load amounts to 9.7 μm, which is far larger than that of the MEMS transducer[14] based on transverse comb-drives.

With our self-developed stiffness calibration setup,[15] the suspending stiffness of the transducer is found to be $k_z = 3.6$ N/m $\pm$ 5% (1σ) and the transducer's resonance frequency f_{MEMS} is about 4.5 kHz. Since $f_{sin} >> f_{MEMS}$, the MEMS movement will not be disturbed by the capacitive sensing system. The sensitivity of the capacitive sensing system of the transducer is 0.2 nm,[15] indicating an indentation force resolution of $\delta F_{indent} = 0.7$ nN. The spring stiffness ratios k_x/k_z and k_y/k_z amount to 53 and 30, respectively, ensuring that this transducer can be used in either the vertical or horizontal orientation without any loss of its functional capability.

For the purpose of material testing, an indenter with an appropriate shape is necessary at the MEMS transducer's main shaft. The MEMS transducer is intended to be used for the characterization of soft materials whose elastic modulus should be generally far lower than that of silicon; a Vickers-like indenter tip is therefore formed directly out of the end of the transducer's

main shaft by means of focused ion beam (FIB) fabrication, as shown in Fig. 2.

The 3D topography of the FIB-made pyramidal tip is thereafter measured by a commercial AFM (Dimension icon®, Bruker Corp.). From this measurement, the projected area function A_p of the silicon tip within its valid indentation depth is evaluated,[16,17] as listed in Table I. The semi-angle of the opposite faces of the pyramidal tip amounts
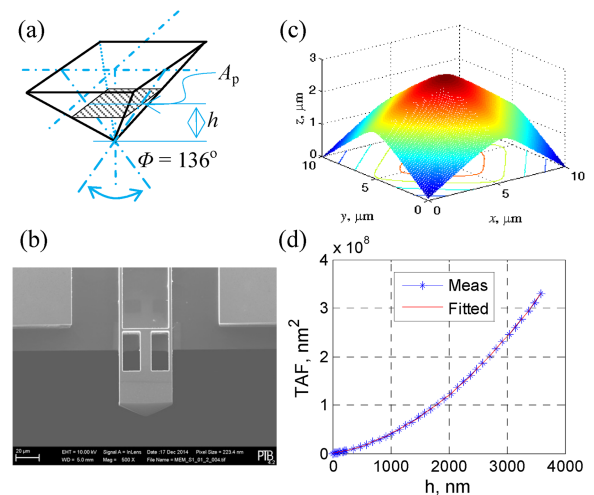

FIG. 2. (a) Schematic diagram of a Vickers indenter tip. (b) Electron microscope image of the FIB-shaped Vickers indenter at the end of the main shaft of the MEMS nanoforce transducer. (c) 3D topography of the FIB-shaped indenter tip measured by an AFM. (d) Tip area function of the FIB-shaped tip evaluated from the AFM image.

TABLE I. A_p coefficients of the FIB-shaped pyramidal tip, where $A_p = \sum\limits_{i=0} c_i \cdot h^{\frac{21-i}{2}}$.

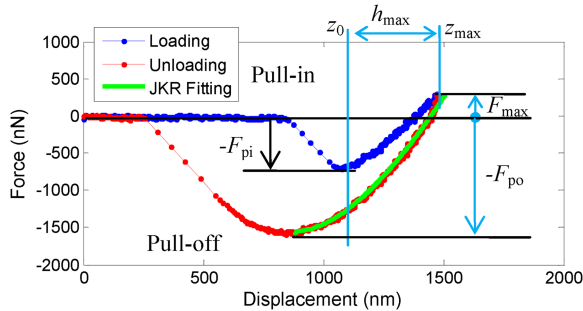| C_0	C_1 (nm)	C_2 (nm$^{3/2}$)	C_3 (nm$^{7/4}$)	C_4 (nm$^{15/8}$)	C_5 (nm$^{31/16}$)
21.5	19 081.5	−17 411.4	10 720.7	7604.7	7083.8

FIG. 3. Typical adhesive force-displacement curve for the PDMS (10:1) sample, where the zero contact point z_0 is obtained by JKR fitting, and the maximum indentation depth $h_{max} = z_{max} - z_0$.

FIG. 4. Measured near-surface elastic modulus E^{JKR} and the work of adhesion W of the sample PDMS (10:1), respectively.

to 68.7° ± 0.2°, well close to its ideal value 68°. As can be seen from Fig. 2(c), the FIB fabricated silicon tip shows evident tip-rounding, with an equivalent tip radius $R_{rounding}$ = 3.96 μm, which leads to a relatively large deviation of C_0 from its ideal value (i.e., 24.5).

To investigate the capabilities of the MEMS nanoindenter, an experimental setup was established, in which a cost-effective three-axis stage integrated with a 3D closed-loop piezo-positioning system (NanoMAX 311, Thorlabs[18]) is used to engage the MEMS transducer and the sample under test.

Within the proof-of-principle tests, the prototype MEMS nanoindenter is employed to determine the mechanical properties of soft polydimethylsiloxane (PDMS), which is one of the most common materials used in microfluidics.[19]

One of the typical force versus displacement curves for the material PDMS (10:1) is shown in Fig. 3, where the pull-in and pull-off phenomena have been clearly revealed. The pull-off force F_{po} for PDMS 10:1 is experimentally determined to be 1543 ± 22 nN (1σ), and the corresponding Tabor parameter μ[20] in our experiments amounts to ≥420. In addition, it should be noted that the relaxation time of typical PDMS samples is usually shorter than 0.5 s;[21] the extremely low loading/unloading rate used in our measurements ensures that no viscoelastic effect has to be considered. Therefore, standard Johnson-Kandall-Roberts (JKR)-model[22]-based data evaluation method practiced in Refs. 21, 23, and 24 can be employed to process the adhesive force-displacement measurement curves.

As illustrated in Fig. 3, the measurement data within the compression segment of the unloading curve[24] is fitted to the JKR model, from which the zero tip-surface contact point z_0 during the unloading procedure, the elastic modulus E^{JKR}, and the work of adhesion W of the PDMS samples can be extracted.
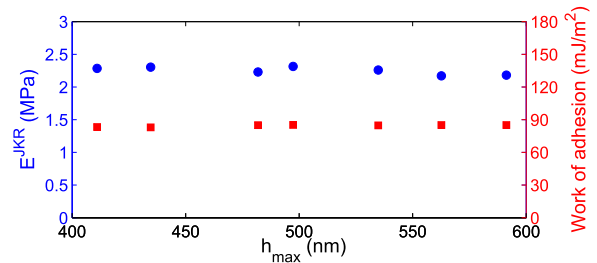
Finally, the measured E^{JKR} and W with respect to the maximum indentation depth h_{max} for PDMS (10:1) are illustrated in Fig. 4. It can be seen that over the shallow indentation range, the sample PDMS 10:1 has $E^{JKR} = 2.3 \pm 0.2$ MPa and $W = 84 \pm 2$ mJ/m^2, respectively. These measurement results are comparable to the values reported in Refs. 21 and 25.

This micro-machined nanoindenter can well bridge the gap between nanoindentation instruments and the AFM-based nanomechanical measurements. Further developments of the MEMS nanoindenter, such as extending the test force up to the mN-range, the functional extension for dynamic measurements, and the integrated fiber interferometer for *in situ* indentation depth measurement, are under consideration.

[1]G. M. Pharr and A. Bolshakov, J. Mater. Res. **17**, 2660–2671 (2002).
[2]ISO 14577-1, "Part 1: Test method," (2002).
[3]B. K. Nowakowski *et al.*, Rev. Sci. Instrum. **84** 075110 (2013).
[4]M. R. VanLandingham *et al.*, Macromol. Symp. **167**, 15–43 (2001).
[5]M. Oyen, J. Mater. Res. **20**, 2094–2100 (2005).
[6]D. C. Lin *et al.*, Biomech. Model. Mechanobiol. **8**, 345–358 (2009).
[7]R. E. Mahaffy, S. Park *et al.*, Biophys. J. **86**, 1777–1793 (2004).
[8]D. Tranchida, Z. Kiflie *et al.*, Meas. Sci. Technol. **20**, 095702 (2009).
[9]D. Passeri, A. Bettucci *et al.*, Rev. Sci. Instrum. **79**, 066105 (2008).
[10]H.-J. Butt *et al.*, Surf. Sci. Rep. **59**, 1–152 (2005).
[11]M. Salerno, Measurement **45**, 2103–2113 (2012).
[12]W. C. Tang *et al.*, Sens. Actuators, A **21**, 328–331 (1990).
[13]K. Hiller *et al.*, Proc. SPIE **5715**, 80–91 (2005).
[14]Y. Oh and S. A. S. Asif, U.S. patent US9,304,072B2 (5 April 2016).
[15]S. Gao *et al.*, Meas. Sci. Technol. **21**, 015103 (2010).
[16]K. Herrman, N. M. Jennett *et al.*, Thin Solid Films **377–378**, 394–400 (2000).
[17]A. C. Barone *et al.*, Microsc. Res. Tech. **73**, 996–1004 (2010).
[18]See www.thorlabs.de/navigation.cfm?guide_id=142 for detailed specifications of this stage.
[19]M. A. Unger, Science **288**, 113–116 (2000).
[20]K. L. Johnson and J. A. Greenwood, J. Colloid Interface Sci. **192**, 326 (1997).
[21]Y.-F. Cao, D.-H. Yang *et al.*, J. Mater. Res. **20**, 2004–2011 (2005).
[22]K. Johnson *et al.*, Proc. R. Soc. London **324**, 301–313 (1971).
[23]O. Pietrement and M. Troyon, J. Colloid Interface Sci. **226**, 166 (2000).
[24]Yu. M. Efremov *et al.*, Colloids Surf., B **134**, 131–139 (2015).
[25]A. Bietsch and B. Michel, J. Appl. Phys. **88**, 4310 (2000).